Elastic Response of Carbon Nanotube Forests to Aerodynamic Stresses

Ilenia Battiato, Prabhakar R. Bandaru, and Daniel M. Tartakovsky*

University of California San Diego, La Jolla, California 92093, USA

The ability to determine static and (hydro)dynamic properties of carbon nanotubes (CNTs) is crucial for many applications. While their static properties (e.g., solubility and wettability) are fairly well understood, their mechanical responses (e.g., deflection under shear) to ambient fluid flow are to a large extent unknown. We analyze the elastic response of single-walled CNT forests, attached to the bottom wall of a channel, to the aerodynamic loading exerted by both laminar and turbulent flows. Our analysis yields analytical expressions for velocity distributions, the drag coefficient, and bending profiles of individual CNTs. This enables us to determine flexural rigidity of CNTs in wind-tunnel experiments. The model predictions agree with laboratory experiments for a large range of channel velocities.

　　　　PACS numbers: 47.56.+r, 62.25.−g

Carbon nanotubes (CNTs) possess a remarkable combination of mechanical characteristics, such as exceptionally high elastic moduli, reversible bending and buckling characteristics, and superplasticity [1]. These properties ensure that complex interactions between fluid flow and patterned nanostructures composed of CNTs play an important role in a variety of applications, including mechanical actuators, chemical filters, and flow sensors [2]. When placed on a body's exterior, CNT "forests" can act as superhydrophobic surfaces that significantly reduce drag [3] thanks to a linear dependence of the slip length on lateral length scales [4]. Observations of fluid flow past CNTs [5] suggest the potential use of CNT forests as sensors of tactile and shear forces.

Predictive and diagnostic capabilities of nanosensors and other nanoforest-covered surfaces are hampered by the relative lack of quantitative understanding of their response to hydro- or aerodynamic loading. Most experiments dealing with these phenomena assemble CNTs into macroscopic sheets or forests. Yet their outcomes (data) are often interpreted with theoretical models that neglect crowding effects by employing the Stokes solution of flow past a single infinite cylinder in either analytical analysis [[5], Eqs. (4) and (7)] or molecular dynamics simulations [[6], Eq. (4)]. Attempts to account for crowding effects by modifying the drag coefficient of each CNT are essentially phenomenological and treat CNTs as infinite cylinders [e.g., [5–7], and references therein].

In this Letter, we predict the elastic response of CNT forests to ambient laminar and turbulent fluid flows and employ these predictions to estimate CNTs' flexural rigidity from the experimental data collected in Ref. [5]. The concept of flexural rigidity is routinely used to forecast the deflection and buckling behaviors of elastic bodies [8], including CNTs. Indeed, their observations of deformations of CNT forests with a scanning electron microscope revealed that *in situ* shearing can be conceptualized as the deflection of a cantilever (Fig. 1).

We develop a closed-form analytical description of fully developed steady-state fluid flow over and through CNT forests, which are used to estimate the average drag coefficient, bending profile, and, ultimately, flexural rigidity of individual CNTs. The incompressible Navier-Stokes equations are used to describe laminar or turbulent flow above the forest, with the porous medium Brinkman equation representing flow through the forest. A viscosity ratio parameter in the Brinkman equation [9] accounts for slip effects at nanotube walls.

A detailed description of the synthesis and patterning of the arrays of vertically aligned, multiwalled CNTs can be found in Ref. [5]. CNTs, with typical heights $H[40–60]$ μm and diameters $2R_0[30–50]$ nm, were grown in square arrays of sizes 5–10 μm on quartz substrates. These CNT forests were placed at the center of a quartz tube with an inner diameter of 6.2 mm at the front edge of the substrate; appropriate measures [5] were taken to prevent the sample vibration or fluid flow entrance effects. The samples were then exposed to fluid (air and argon) at various pressures, and fluid velocities were calibrated by using the flow chamber cross-sectional area and volumetric flow rates as measured by a flow meter. A linearly polarized He-Ne laser ($\lambda = 633$ nm) was used to illuminate the CNT forests, and the transmitted light intensity was monitored as a function of fluid flow. As the axis of the polarizer
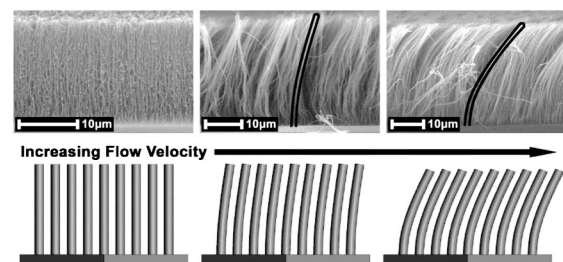

FIG. 1. Scanning electron microscope imaging of *in situ* shearing of CNT forests and their representation with a cantilever [after Ref. [5]].
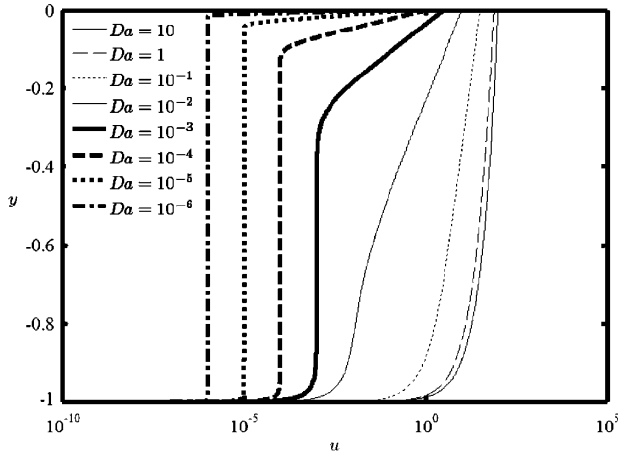
FIG. 2.   Laminar regime: Dimensionless velocity profile $u(y)$ inside the CNT forest for $M = 1$, $\epsilon = 0.001$, $\delta = 100$, and several values of the Darcy number Da.

was initially oriented parallel to the laser polarization direction, the deflections of the CNT ensembles (initially oriented parallel to the polarized laser beam) were translated into a change of the light intensity and sampled by a photodetector or a CCD camera. Multiple measurements and averaging of the obtained deflections lowers the error in the recorded deflections; e.g., at the upper air velocity limit of ≈ 65 m/s, the displacement error on the order of ± 0.5 μm was observed.

To model the experiment, we consider a fully developed incompressible fluid flow between two infinite parallel plates separated by the distance of $H + 2L$. The bottom part of the flow domain, $-H < \hat{y} < 0$, is occupied by square-patterned arrays of CNTs with the midway distance between aligned nanotubes R_1. The remainder of the flow domain, $0 < \hat{y} < 2L$, is occupied by a free fluid. The flow is driven by an externally imposed (mean) constant pressure gradient $dp/dx < 0$.

We treat the CNT forest (the region occupied by CNTs, $\hat{y} \in [-H, 0]$) as a porous medium with permeability K and porosity $\phi = 1 - (R_0/R_1)^2$ and employ the Brinkman equation [9] to describe a distribution of the horizontal component of the intrinsic average velocity u in this region:

$$M\frac{d^2u}{dy^2} - \frac{u}{\text{Da}} + 1 = 0, \qquad y \in (-1, 0). \quad (1)$$

In this dimensionless form of the Brinkman equation, flow velocity $\hat{u}$ is normalized with a characteristic Darcy velocity $q = -(H^2/\mu)dp/dx$, i.e., $u = \hat{u}/q$; the vertical coordinate is scaled with the CNT height $y = \hat{y}/H$; $M = \mu_e/\mu$ denotes the ratio of the fluid's dynamic viscosity μ and its "effective" counterpart μ_e, which accounts for the slip at the CNT walls; and $\text{Da} = K/H^2$ is the Darcy number. Since the experimentally observed maximum bending of the CNTs is about 10% of their length, we assume that bending has a negligible effect on permeability. This allows us to decouple an analysis of the flow from that of the mechanics

of the bending. This assumption is validated below by comparing the model predictions with experimental data.

In the rest of the flow domain, $\hat{y} \in (0, 2L)$, we use dimensionless forms of either the steady-state Stokes or steady-state Reynolds equations to describe fully developed flow, respectively, in either laminar ($\gamma = 0$) or turbulent ($\gamma = 1$) regimes [[10], Eqs. (7) and (8)]:

$$\frac{d^2u}{dy^2} - \gamma \text{Re}_p \frac{d\langle \tilde{u}\, \tilde{v} \rangle}{dy} + 1 = 0, \qquad y \in (0, 2\delta). \quad (2)$$

In (2), $\text{Re}_p = \rho H q/\mu$ is the Reynolds number for porous flow of a fluid with density ρ, $\delta = L/H$, and $u(y)$ is the dimensionless horizontal component of the normalized flow velocity $\mathbf{u}(u, v)$. In the laminar regime, u is the actual velocity and $v \equiv 0$. In the turbulent regime, $\mathbf{u}$ denotes the mean velocity, dp/dx is the mean pressure gradient, $\tilde{u}$ and $\tilde{v}$ are the velocity fluctuations about their respective means, and $\langle \tilde{u}\, \tilde{v} \rangle$ is the Reynolds stress. Fully developed turbulent channel flow has velocity statistics that depend on y only.

In both flow regimes, the no-slip condition $u = 0$ is imposed at the channel surfaces $y = -1$ and $y = 2\delta$, and the continuity of velocity and shear stress is prescribed at the interface $y = 0$ between the free and filtration flows:

$$u(0^-) = u(0^+) = U, \qquad M\frac{du}{dy}(0^-) = \frac{du}{dy}(0^+), \quad (3)$$

where $U = \hat{U}/q$ is an unknown dimensionless matching velocity.

The permeability of the CNT forest, represented here by square arrays of vertical cylinders, is related to porosity ϕ by Eq. (19) in Ref. [11]. Its dimensionless form allows us to express the Darcy number Da in terms of porosity ϕ and the geometric factor $\epsilon = R_1/H$ as $\text{Da} = -\epsilon^2/8\{\ln(1 - \phi) + [(1 - \phi)^{-2} - 1]/[(1 - \phi)^{-2} + 1]\}$. Hence $\text{Da} \ll 1$ for $\epsilon < 1$ regardless of the magnitude of ϕ. This implies that crowding effects cannot be neglected for arrays of obstacles, whose geometric ratio $\epsilon \lesssim 1$. Even in high porosity CNT forests ($\phi \approx 0.8$–0.9), common values of $\epsilon \approx 10^{-2}$–10^{-3} give rise to $\text{Da} \approx 10^{-5}$–$10^{-7}$.

A solution of (1)–(3) with $\gamma = 0$ yields a velocity profile in the laminar regime:

$$u(y) = \begin{cases} \text{Da} + C_1 e^{\lambda y} + C_2 e^{-\lambda y}, & y \in [-1, 0], \\ -y^2/2 + [\delta - U/(2\delta)]y + U, & y \in [0, 2\delta], \end{cases} \quad (4)$$

where $\lambda = 1/\sqrt{M\text{Da}}$, $C_1 = [(U - \text{Da})e^\lambda + \text{Da}]/(e^\lambda - e^{-\lambda})$, and $C_2 = -[(U - \text{Da})e^{-\lambda} + \text{Da}]/(e^\lambda - e^{-\lambda})$. The interfacial velocity U is given by

$$U = \text{Da}\frac{1 - \text{sech}\lambda}{\beta} + \frac{\delta}{\lambda M}\frac{\tanh\lambda}{\beta}, \quad (5)$$

where $\beta = 1 + (\tanh\lambda)/(2\delta\lambda M)$. Figure 2 presents the resulting velocity profiles in the CNT forest for $M = 1$, $\epsilon = 0.001$, $\delta = 100$, and several values of the Darcy number Da. For small values of Da, when the crowding of CNTs becomes pronounced, the velocity profile is characteristic of plug flow everywhere in the CNT forest, except in the vicinity of the CNT tips.

To obtain a mean velocity profile in the turbulent regime, we solve (1)–(3) with $\gamma = 1$ by assuming the top of the CNT forest to be hydrodynamically smooth. Then the dimensionless mean velocity $u(y)$ in the viscous sublayer of dimensionless width δ_μ obeys the "law of the wall" [[10], pp. 270–271]: $u = \delta y + U$ for $y \in [0, \delta_\mu]$. The interfacial velocity U is now given by (5) with $\beta = 1$. Thus, the interfacial velocities U in the laminar and turbulent regimes differ only by the factor of β. One can verify that $\beta \rightarrow 1$ as the Darcy number $\mathrm{Da} \rightarrow 0$, i.e., when the permeability and porosity of CNT forests become small. These conditions are satisfied in the experimental setup in Ref. [5], where $\mathrm{Da} \approx 10^{-5}$–$10^{-7}$.

The drag force per horizontal unit area exerted by the fluid on any cross section $y = \mathrm{const}$ of the CNT forest is given by the xy component of the stress tensor $\hat{\sigma}_{xy} = \mu_e d\hat{u}/d\hat{y}$. The drag force distribution along an individual CNT, $\hat{\mathcal{D}}(\hat{y})$, is obtained by dividing $\hat{\sigma}_{xy}$ with the number of CNTs per unit length, $\mathcal{N} = 1/R_1$. Its dimensionless form is $\mathcal{D} = \epsilon M du/dy$, wherein $u(y)$ is given by the first expression in (4). The total dimensionless drag force exerted by the fluid on the CNT is $\mathcal{F} = \epsilon M U$, and its dimensional counterpart is $\hat{\mathcal{F}} = R_1 \mu_e \hat{U}$. Defining a drag coefficient C_D as the ratio between $\hat{\mathcal{F}}$ and $A\rho q^2/2$, where $A = 2R_0 H$ is the CNT surface area projected onto a plane normal to the velocity vector, we obtain

$$C_D = \frac{1}{\mathrm{Re}_p} \frac{MU}{\sqrt{1 - \phi}}. \qquad (6)$$

Equation (6) expresses the drag coefficient of an individual CNT in terms of the porosity of a CNT forest ϕ, the Reynolds number for the porous flow Re_p, and the dimensionless velocity at the interface separating the free and porous flows. To the best of our knowledge, this is the first rigorously derived formula for the drag coefficient for arrays of *finite* cylinders under *nonuniform* flow conditions. Previous results hold for infinite cylinders or spheres in a velocity field that is uniform on average.

The dimensionless drag force $\mathcal{D}(y)$ exerted by the fluid on a CNT causes its horizontal dimensionless deflection $l(y)$, with $l = \hat{l}/H$ and $\hat{l}$ denoting the dimensional deflection. By treating an elastic CNT with the Young modulus $\hat{E}$ as a cantilever and denoting its moment of inertia by $\hat{I}$, the deflection $l(y)$ can be found [5,12] as a solution of

$$\frac{d^2}{dy^2}\left(EI\frac{d^2l}{dy^2}\right) = \epsilon M \frac{du}{dy}, \qquad y \in (-1, 0), \qquad (7)$$

where the product EI defines the dimensionless flexural rigidity of an CNT ensemble: $EI = \hat{E}\hat{I}/(H^3\mu q)$. At the CNT's fixed end $y = -1$, both the deflection (l) and its slope (dl/dy) are zero. The shear (d^2l/dy^2) at and bending moment (d^3l/dy^3) of the CNT's free end $y = 0$ are both zero. Equation (7) subject to these boundary conditions can be readily integrated in closed form, leading to the CNT bending profiles shown in Fig. 3.

The experimental data reported by Ref. [5] consist of measurements of deflection of the CNT tips, $\hat{X} = \hat{l}(0)$, for a given bulk velocity across the wind tunnel $\hat{u}_b$. The experiments were conducted in turbulent regimes and were used to estimate the flexural rigidity $\hat{E}\hat{I}$ of five CNT samples, whose length $\hat{H}$ ranged from 40 to 60 μm.

Let us define a dimensionless bulk velocity across the wind tunnel as

$$u_b = \frac{1}{1 + 2\delta}\int_{-1}^{2\delta} u(y)dy, \qquad (8)$$

with $\hat{u}_b = u_b q$. Substituting the first equation in (4) into (8), we obtain

$$u_b = \frac{Q}{1 + 2\delta} + \frac{2\delta}{1 + 2\delta}u_{\mathrm{av}}, \qquad u_{\mathrm{av}} = \frac{1}{2\delta}\int_0^{2\delta} u(y)dy, \qquad (9)$$

where $Q = \mathrm{Da} + (U - 2\mathrm{Da})(\coth\lambda - \mathrm{csch}\lambda)/\lambda$ is the flow rate through the CNT forest. We find u_{av} in the turbulent regime by assuming that the effects of the slip velocity U on u_{av} are negligibly small. This allows us to employ a relationship between the friction velocity $\hat{u}_\tau \equiv \sqrt{-(L/\rho)dp/dx}$ and the average bulk velocity $\hat{u}_{\mathrm{av}}$ of turbulent flow in a channel of width $2L$ [[10], p. 278], whose dimensionless form is

$$1 + u_{\mathrm{av}}\kappa\sqrt{\mathrm{Re}_p/\delta} = \ln\sqrt{\delta^3\mathrm{Re}_p} + 5.9\kappa, \qquad (10)$$

where $\kappa = 0.41$ is the von Kármán constant. The combination of (9) and (10) allows one to determine the Darcy velocity q from measurements of the average bulk velocity $\hat{u}_b$.

Data sets collected by Ref. [5] consist of measurement pairs $(\hat{u}_b, \hat{X})$. The relevant parameters used in these experiments are $R_0 = 0.02$ μm, $R_1 = 0.08$ μm, $H = 40$–60 μm, $L = 1.5$ mm, $K = 1.4 \times 10^{-3}$ μm^2, $\rho_{\mathrm{air}} = 1.2$ kg/m^3, $\rho_{\mathrm{Ar}} = 1.784$ kg/m^3, $\mu_{\mathrm{air}} = 1.8 \times 10^{-5}$ kg/(ms), $\mu_{\mathrm{Ar}} = 2.1 \times 10^{-5}$ kg/(ms), and $\hat{u}_b = 5$–55 m/s. They give rise to dimensionless parameters $\phi = 0.97$, $\mathrm{Da} = 3.94$–8.86×10^{-7}, $\delta = 24.83$–37.75, $M = 1$, and $\epsilon = 1.3$–2×10^{-3}. We use measurements of average bulk velocity $\hat{u}_b$ to determine the
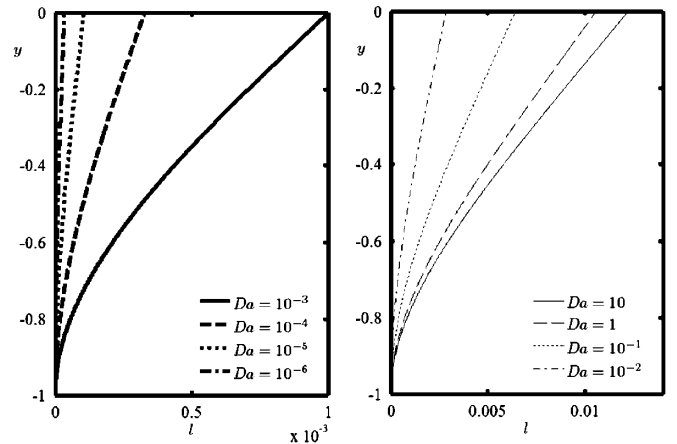

FIG. 3.   Dimensionless CNT bending profiles for $M = 1$, $\epsilon = 0.001$, $\delta = 100$, U given by (5), and several values of Da.
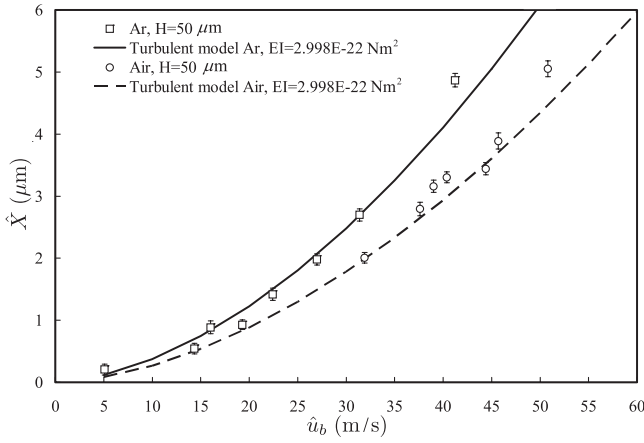
FIG. 4.   Experimental (symbols) and predicted (lines) deflections of the CNT tip $\hat{X}$ in response to hydrodynamic loading by the turbulent flows of argon (squares) and air (circles) for a range of the bulk velocity values $\hat{u}_b$. The data from Ref. [5] are for CNTs of height $\hat{H} = 50$ μm.

scaling factor (Darcy velocity) q and measurements of the deflection of a CNT's tip $\hat{X}$ to estimate the flexural rigidity $\hat{E}\hat{I}$ of CNTs as

$$\hat{E}\hat{I} = \mu q H^4 [2I_4(0) + B/3]/(2\hat{X}), \qquad (11)$$

where $B = 2I_1(0) - 3I_2(0) - 6I_3(-1) - 6I_4(-1)$ and $I_n(y) = \epsilon M \lambda^{1-n}[C_1 e^{\lambda y} + (-1)^{n+1} C_2 e^{-\lambda y}]$ for $n = 1, \ldots, 4$. Equation (11) provides a closed-form expression to estimate the flexural rigidity of carbon nanotubes from their elastic response to hydrodynamic loading. We used (11) to determine $\hat{E}\hat{I}_{\mathrm{av}}$ for each sample, with the average flexural rigidity among all samples 2.68×10^{-22} N m^2.

Alternatively, for a known value of $\hat{E}\hat{I}$, (11) can be used to predict the CNT tip deflections due to hydrodynamic loading of CNTs caused by different fluids and/or various values of average bulk velocity $\hat{u}_b$. Such predictions serve to validate our model through comparison with the experiments of Ref. [5]. Figure 4 presents experimental data and model predictions based on (11) wherein the average value of the CNT flexural rigidity, $\hat{E}\hat{I}_{\mathrm{av}} = 2.99 \times 10^{-22}$ Nm^2, is computed from experiments with argon and then used to predict CNT deflections for air flow. The figure reveals good agreement between theory and experiment over a wide range of flow velocities. Although not shown here, similarly good agreement was observed for other CNT heights. For large velocities ($\hat{u}_b \geq 45$ m/s), the assumptions of elastic bending and constant permeability of a CNT forest may be violated because CNTs can overlap and develop kinks.

A typical wall thickness of CNTs with diameter $2R_0 = 40$ nm is 0.34 nm, which corresponds to the second moment of inertia $I \approx 8.3 \times 10^{-33}$ m^4. Hence our estimates of the flexural rigidity EI predict the Young modulus of individual CNTs to be $E \approx 0.034$ TPa, which is of the same order of magnitude as $E \approx 0.09$ TPa reported in Ref. [13] [Fig. 3(a)] for single CNTs of comparable diame-

ters. The factor of 3 discrepancy between the Young moduli of a single CNT and assembled CNTs is to be expected. Indeed, the latter often exhibit moduli that are more than an order of magnitude lower than the intrinsic moduli of individual nanotubes. This phenomenon has been attributed to growth techniques where impurities coat the surface of nanotubes and to the formation of bundles of parallel tubes, which reduce the effective surface area available for shear transfer [14].

In conclusion, this Letter sheds new light on CNT-fluid flow interactions by going beyond phenomenological approaches, which fit data from physical experiments [5] and/or molecular dynamics simulations [6] to the Stokes solution for flow past a single infinite cylinder. Unlike these and other similar analyses [e.g., [7]], our model accounts for the effects of both crowding in CNT forests and their finite height. This is accomplished by treating CNT forests as a porous medium and deriving analytical solutions for a coupled system of the Navier-Stokes and Brinkman equations, which describe flow over and through CNT forests, respectively. This yields closed-form expressions for the drag force exerted on individual CNTs, the corresponding drag coefficient C_D, and the bending profile of individual CNTs. To the best of our knowledge, this is the first rigorously derived expression for C_D, which takes into account the compound effects of both crowding in CNT forests and their finite height. The deflection of their tips can serve to estimate the flexural rigidity of CNTs. We demonstrated good agreement between our model predictions and experimental data.

*dmt@ucsd.edu

[1] M. M. J. Treacy, T. W. Ebbesen, and J. M. Gibson, Nature (London) **381**, 678 (1996); M. R. Falvo *et al.*, Nature (London) **389**, 582 (1997); J. Y. Huang *et al.*, Nature (London) **439**, 281 (2006).
[2] P. Kim and C. M. Lieber, Science **286**, 2148 (1999); S. Ghosh, A. K. Sood, and N. Kumar, Science **299**, 1042 (2003).
[3] M. Wilson, Phys. Today **62**, 16 (2009).
[4] P. Joseph *et al.*, Phys. Rev. Lett. **97**, 156104 (2006).
[5] C. Deck *et al.*, J. Appl. Phys. **106**, 074304 (2009).
[6] J. H. Walther *et al.*, Phys. Rev. E **69**, 062201 (2004).
[7] A. Ford and D. Papavassiliou, Ind. Eng. Chem. Res. **45**, 1797 (2006).
[8] F. P. Beer, J. E. R. Johnson, and J. T. De Wolf, *Mechanics of Materials* (McGraw-Hill, Boston, 2006), 4th ed.
[9] F. Valdes-Parada, J. Ochoa-Tapia, and J. Alvarez-Ramirez, Physica (Amsterdam) **385A**, 69 (2007).
[10] S. B. Pope, *Turbulent Flows* (Cambridge University Press, New York, 2000).
[11] J. Happel, AIChE J. **5**, 174 (1959).
[12] S. Weinbaum *et al.*, Proc. Natl. Acad. Sci. U.S.A. **100**, 7988 (2003).
[13] P. Poncharal *et al.*, Science **283**, 1513 (1999).
[14] R. Baughman, A. A. Zakhidov, and W. A. de Heer, Science **297**, 787 (2002).